11th International Conference
1-3 July 2013
Pisa
RASD 2013

UNDERSTANDING HOW KURTOSIS IS TRANSFERRED FROM INPUT ACCELERATION TO STRESS RESPONSE AND ITS INFLUENCE ON FATIGUE LIFE

Frédéric Kihm[1*], Stephen A. Rizzi[2], Neil S. Ferguson[3] and Andrew Halfpenny[1]
[1]HBM-nCode Products Division
Technology Center, Brunel Way, Catcliffe
Rotherham, S60 5WG, UK
E-mail: frederic.kihm@hbmncode.com, andrew.halfpenny@hbm.com

[2]NASA Langley Research Center
Structural Acoustics Branch
Hampton, Virginia 23681 USA
E-mail: Stephen.A.Rizzi@nasa.gov

[3]Institute of Sound and Vibration Research
University of Southampton
Southampton SO17 1BJ, UK
E-mail: nsf@isvr.soton.ac.uk

Keywords: kurtosis, non-Gaussian, fatigue, vibration, linear filter.

ABSTRACT

High cycle fatigue of metals typically occurs through long term exposure to time varying loads which, although modest in amplitude, give rise to microscopic cracks that can ultimately propagate to failure. The fatigue life of a component is primarily dependent on the stress amplitude response at critical failure locations. For most vibration tests, it is common to assume a Gaussian distribution of both the input acceleration and stress response. In real life, however, it is common to experience non-Gaussian acceleration input, and this can cause the response to be non-Gaussian. Examples of non-Gaussian loads include road irregularities such as potholes in the automotive world or turbulent boundary layer pressure fluctuations for the aerospace sector or more generally wind, wave or high amplitude acoustic loads.

The paper first reviews some of the methods used to generate non-Gaussian excitation signals with a given power spectral density and kurtosis. The kurtosis of the response is examined once the signal is passed through a linear time invariant system. Finally an algorithm is presented that determines the output kurtosis based upon the input kurtosis, the input power spectral density and the frequency response function of the system. The algorithm is validated using numerical simulations. Direct applications of these results include improved fatigue life estimations and a method to accelerate shaker tests by generating high kurtosis, non-Gaussian drive signals.

1. INTRODUCTION

Any operational loads monitoring exercise will show that loads differ from one application to another. Some loadings, like shocks, are of a transient nature, while others, like turbulent boundary layer, are of a random nature. A random process can be stationary or non-stationary, Gaussian or non-Gaussian. A process is referred to as 'stationary' if its probability distribution does not change with respect to time. A random variable x is said to be Gaussian if its probability density function (PDF) is given by

$$P_X(x) = \frac{1}{\sqrt{2\pi\sigma^2}} e^{-\frac{(x-\mu)^2}{2\sigma^2}} \tag{1}$$

where μ is the mean and σ is the standard deviation.

A non-stationary process is often represented as a signal with time-varying variance. Gust loading is an important part of the fatigue induced on an aircraft structure. In this case, gusts with various amplitudes and directions must be considered. Similarly, road irregularities and vehicle speed variations are the primary cause of failure in automotive structures and components. Both gust loading and road irregularities can be represented by signals with time-varying variance.

It is desirable for a design engineer or a test technician to have the means to compute the kurtosis of the stress responses at critical locations of a component or structure. This would allow the design engineer to perform more accurate fatigue life estimations using a spectral fatigue approach and the test technician to know the acceleration factor that can be achieved by using the existing kurtosis control capabilities of a shaker.

Kurtosis is one of the principal metrics describing non-Gaussian features of a unimodal probability distribution. It is often described as a measure of the "peakedness" of a process . The kurtosis is calculated from the fourth central moment (m_4) of a random variable x, normalized by the square of the variance (m_2), i.e.,

$$\kappa = \frac{m_4}{m_2^{\,2}}, \quad m_j = \frac{1}{n}\sum_{i=1}^{n} \left[x_i - \mu \right]^j \tag{2}$$

Kurtosis of a Gaussian distribution is 3.0. A process is said to be leptokurtic if its kurtosis is higher than 3.0, and platykurtic if smaller than 3.0.

In recent work by Rizzi et al. [1], it was found that a leptokurtic loading having a steady rate of instantaneous, high-excursion peaks produced essentially the same response as if the load was Gaussian. In contrast, the response to a non-Gaussian loading having the same kurtosis, but with bursts of high values was found to be non-Gaussian and also leptokurtic. Over a practical range of damping, it was found that the linear response to a non-Gaussian loading was Gaussian when the period of the system impulse response is much greater than the rate of the peaks in the loading. A lower damping would typically reduce the excess kurtosis in the response.

In this paper the previous study is further extended by concentrating more on stresses and fatigue damage. Also, the processes for simulating a non-Gaussian signal are more fully discussed. A formulation is proposed that gives the statistics of the response due to a steady non-Gaussian loading. Finally, the case of non-Gaussian loading with bursts of high amplitude excursions is further explored and the relationship between the system impulse response and the frequency at which the bursts occur in the loading is illustrated.

2. SIGNAL GENERATION

In the following sections, three forms of loading signal generation are undertaken: Gaussian, a non-Gaussian form using a PDF transform approach, and a non-Gaussian form using amplitude modulation.

2.1 Gaussian stationary signal generation

Time histories corresponding to particular power spectral densities (PSD) may be generated in various manners. One method is based on time domain filtering of white noise. In this case, the coefficients of the finite impulse response filter are calculated from an amplitude specified by the square root of the PSD, and a phase specified by a uniform random distribution between [-π, π].

Another method of signal generation is based on the inverse Fourier transform (IFT) of a frequency domain signal constructed with an amplitude specified by the PSD combined with a random phase. Newland [2] expresses the time signal reconstruction of a stationary, zero-mean process as:

$$x(t) = Re\left(\sum_{k=0}^{N-1} \sqrt{2\Delta f\, G_{XX}(k\Delta f)}\, e^{2i\pi kt\Delta f}\, e^{i\varphi_k}\right) \tag{3}$$

with G_{xx} the PSD to be inverted, φ the randomized phase between [-π, π], Δf the frequency resolution and N the number of frequency lines.

The length and sample rate of the signal generated depend on the frequency resolution and the maximum frequency of the PSD respectively. Note that the signal obtained with the IFT method is generally considered as having a lower level of randomness than filtered white noise [3]. For instance a filtered white noise is expected to be unbounded, whereas the maximum of a signal obtained with the IFT method is limited as shown by:

$$\max\left(x(t)\right) \le \sum_{k=0}^{N-1} \sqrt{2\Delta f\, G_{XX}(k\Delta f)} \tag{4}$$

An extension of the previous method for generating a colored Gaussian process is the so-called 'inverse Welch' method, as it was modeled after the Welch method for estimating spectral density [3]. Frames of random data obtained from the IFT method are multiplied by a window, overlapped, and added to form a nearly stationary output. The weighting windows allow continuous frequency content and help limit leakage. A typical window is the Hanning window. The level of overlap dictates whether the resulting signal will be stationary or not. For instance, Hanning windows, which are essentially cosine functions, when overlapped by 67% will provide a uniform statistical weighting which in turn will generate a stationary signal. Figure 1 shows a target PSD overlaid with the PSD of the signals obtained after filtering white noise and using the inverse Welch method.

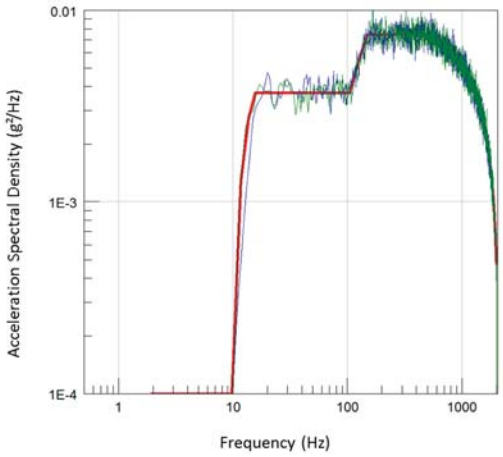

Figure 1: Comparison of prescribed PSD (red) with PSD of generated signals using the white noise filtering (blue) and inverse Welch (green) approaches.

Both the filtered white noise and the inverse Welch approaches give very similar and satisfactory results. The inverse Welch method is adopted here because it offers more flexibility, particularly when non-stationary signal generation is required.

2.2 Steady non-Gaussian signal generation - PDF transform technique

The technique introduced in this section can be used to obtain a non-Gaussian stationary signal, showing a steady rate of instantaneous peaks.

The PDF of a random variable x can be transformed to the PDF of a different random variable z using the PDF transform [4, 5]:

$$P_Z(z) = \frac{P_X(x)}{\left| dz/dx \right|} \tag{5}$$

where there is a one-to-one monotonic relationship between x and z, that is, $z = g(x)$. Several formulae for the transformation g(.) have been proposed in the literature [6, 7]. The idea is based on the fact that squaring part of a Gaussian signal will have the effect of skewing it, whereas cubing a Gaussian signal will make it leptokurtic. Several authors [6, 7] thought of using a polynomial transform of the general form:

$$Z = c + \alpha X + \beta X^2 + \gamma X^3 \tag{6}$$

with c, α, β and γ coefficients driving the type and amount of non-Gaussianity that is required. Typically, the constant c in equation (6) specifies the mean value, while α drives the standard deviation of Z. The β and γ coefficients influence the skewness and kurtosis respectively. The goal is therefore to find a relationship between the coefficients in equation (6) and the required statistics for Z.

Winterstein [6] considered using Hermite polynomials to expand a Gaussian PDF to match the first statistical moments required of the transformed signal z. For a leptokurtic process, Winterstein's model [6, 8] defines the direct transformation g that allows one to obtain $z(t)$ from $x(t)$ as:

$$z = \mu_X + \sigma_X K \left[\frac{x}{\sigma} + \tilde{h}_3 \left(\frac{x}{\sigma} - 1 \right) + \tilde{h}_4 \left(\left(\frac{x}{\sigma} \right)^3 - 3\frac{x}{\sigma} \right) \right] \tag{7}$$

with:

$$K = \frac{1}{\sqrt{1 + 2\tilde{h}_3^{\,2} + 6\tilde{h}_4^{\,2}}} \quad , \quad \tilde{h}_3 = \frac{\gamma_3}{6(1 + 6\tilde{h}_4)} \quad , \quad \tilde{h}_4 = \frac{\sqrt{1 + 1.5(\gamma_4 - 3)} - 1}{18}$$

where γ_3 and γ_4 are the expected skewness and expected kurtosis respectively. The Winterstein model was adopted here for the generation of steady non-Gaussian signals because it appears to be widely accepted and it is known to provide an accurate representation of a wide range of nonlinear behaviours [8]. Note that this method has one major drawback: it introduces harmonic distortions which reduce the dynamic range in the spectral density of the generated data [9].

2.3 Burst non-Gaussian signal generation - amplitude modulation technique

Another class of high kurtosis random signals is made of non-stationary processes. Although vibration is generally of random form, it is often non-stationary. In the automotive world, this arises from changes in road surface quality and vehicle speed. A non-stationary process can be represented as a signal with time-varying variance, typically obtained through a modulation process.

The process for generating a non-Gaussian signal with bursts starts with the generation of a stationary Gaussian signal. This signal is then amplitude modulated by a low frequency carrier wave, independent of the Gaussian signal. In order to create the large excursions, the amplitude of each cycle of the carrier wave is a random variable. As described by Smallwood in [3], a β distribution is chosen for the realizations of the random variable. The β distribution is chosen because it generates only positive values and is extremely flexible. The mean value of the distribution is fixed to 1.0, while its variance is used to control the kurtosis. Note that the skewness obtained using this method is zero.

The non-Gaussian signal $z(t)$ can therefore be written $z(t) = a(t).x(t)$, where $a(t)$ is a amplitude modulation coefficient that changes over time and $x(t)$ are realizations of a stationary Gaussian process. The bursts that are created in the resulting signal occur at a given rate, which derives from the period of the modulating signal $a(t)$. Also, the statistics of $z(t)$ can be derived from the statistics of the independent signals $a(t)$ and $x(t)$.

It is therefore possible to construct a burst non-Gaussian loading with a prescribed PSD and kurtosis value by generating two signals that are multiplied. First, a Gaussian stationary signal is generated from the given PSD. Secondly, a low frequency varying amplitude carrier wave is constructed. The amplitudes of the waves generated in this study are realizations of a β distribution with parameters carefully chosen such that the kurtosis of the wave is one third of the required kurtosis. Finally, the resulting signal is obtained by multiplying both signals and then scaling to the original RMS value. Such a burst non-Gaussian signal is illustrated in Figure 2.

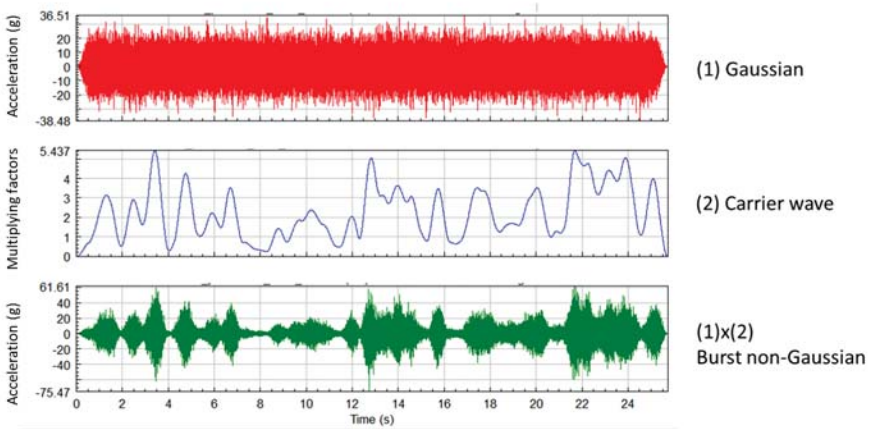

Figure 2: Construction of a burst non-Gaussian signal

3. NUMERICAL SIMULATIONS: LINEAR TIME-INVARIANT SYSTEM

The response kurtosis, maximum stress and fatigue damage for a simple, but realistic, engineering structure is next considered to demonstrate how these quantities change for non-Gaussian loadings with the same kurtosis but with differing temporal character.

3.1 The Finite Element model, boundary conditions and material properties

The engineering structure considered is an off-the-shelf automotive horn bracket. The finite element model of the bracket is shown in Figure 3. The bracket was modelled with the finite element analysis program ABAQUS [10]. The bracket is constructed with 168 S3R and 5382 S4R shell elements. Two lumped masses representing the horns were constructed with 8074 C3D4 constant stress tetrahedron solid elements. Different mass values can simulate asymmetry of the weight distribution. The bracket was constructed from carbon steel, with the properties indicated in Table 1.

The fatigue S-N curve, when plotted on a log-log scale, is specified by a line with constant slope, and no fatigue limit. Under simulated test, the specimen is clamped to the test rig at the left end and excited in the transverse direction, as shown in Figure 3. The following section describes the applied loading.

3.2 Input signal generation

The prescribed acceleration PSD, shown in Figure 4, originates from MIL-STD-810F [11]. The loading has a frequency range of 10-2000 Hz and an amplitude of 3.7g RMS.

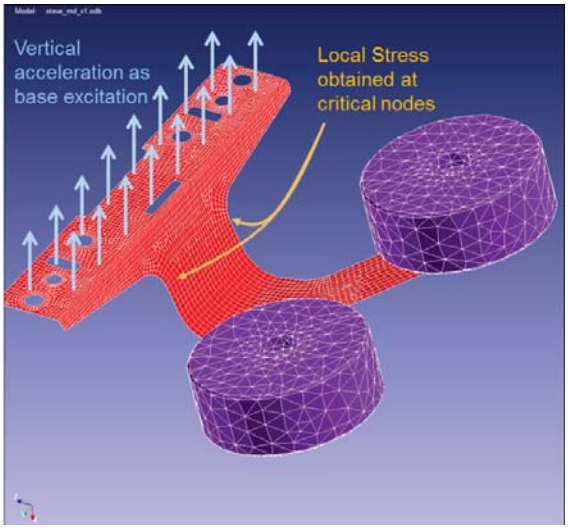

Figure 3: The finite element model of the bracket with boundary conditions.

	Property	Value
Mechanical properties	Young Modulus	210 GPa
	Density	7890 kg/m^3
	Modal damping	0.025
	Yield Stress	400 MPa
	Ultimate tensile strength	700 MPa
Fatigue properties	Basquin slope	14
	Stress Range Intercept	1200 MPa

Table 1: Material properties of horn bracket.

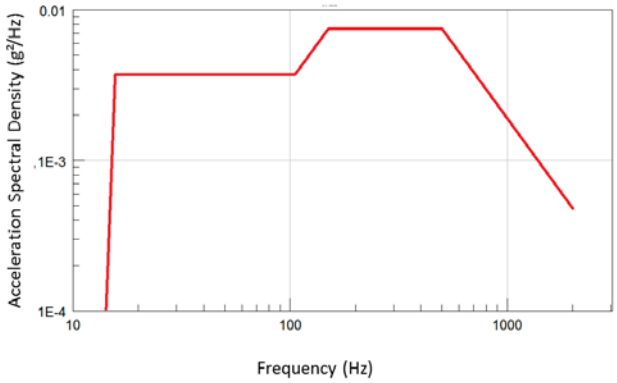

Figure 4: The excitation PSD used for Gaussian and non-Gaussian loadings.

Three different excitation signals were produced from this PSD. The first one is a stationary Gaussian signal, whereas the other two are leptokurtic with a high kurtosis value of roughly 7. All signals share the same PSD and therefore the same RMS value. The first leptokurtic signal was obtained by the PDF transform as described in section 2.2, while the latter results from the amplitude modulation described in section 2.3. For the latter, the modulator is made of a series of 50% overlapped Hanning windows, each comprised of 1024 points. All signals are 50 seconds in duration and are sampled at 4096 samples per second. The signals and their PDFs are illustrated in the Figure 5 and Figure 6. In Figure 5, the steady rate of high amplitude peaks is shown in the non-Gaussian signal generated using the PDF transformed technique, whereas the signal generated with the amplitude modulated approach shows bursts. The same kurtosis for both non-Gaussian signals is clearly seen in the PDFs in Figure 6.

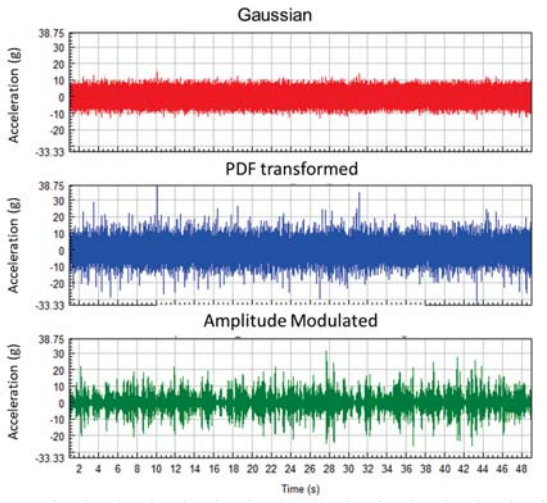

Figure 5: The excitation signals generated: Gaussian (red), steady non-Gaussian using PDF transform method (blue) and burst non-Gaussian using amplitude modulation method (green).

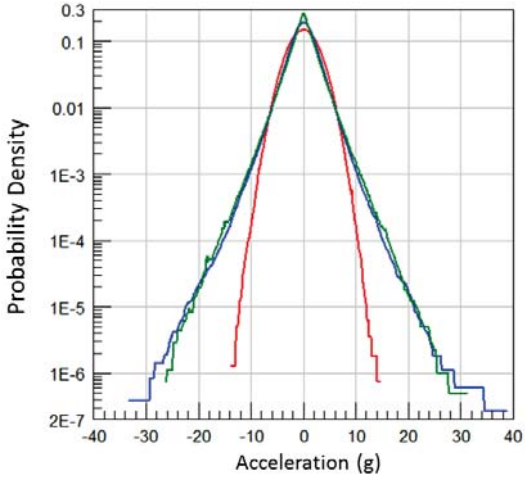

Figure 6: The PDFs of the excitation signals: Gaussian (red), steady non-Gaussian (blue) and burst non-Gaussian (green).

3.3 Dynamic finite element analyses

Two linear dynamic response analyses were performed via the finite element method: a forced frequency response analysis and a transient analysis. Results from the forced frequency response analysis serve as input to a spectral fatigue calculation, while results from the transient analysis serve as input to a fatigue analysis performed using time domain data and a rainflow cycle [12] counting scheme.

The forced frequency response analysis was performed by exciting the structure in physical degrees-of-freedom with a 1 g vertical sinusoidal base acceleration input over the frequency range of interest. The resulting frequency response function (FRF) between the loading and the response is obtained in this manner. An example FRF for the absolute maximum principal stress (Pa/g) is shown in Figure 7 for the critical node 3100 (see Figure 10). The absolute maximum principal stress is defined as the principal stress with the largest magnitude. Once the FRF is known, the response PSD G_{YY} can be calculated for any loading PSD G_{XX} as:

$$G_{YY}(\omega) = \left|H(\omega)\right|^2 \cdot G_{XX}(\omega) \tag{8}$$

where $H(\omega)$ represents the FRF. For the fatigue analysis, stress cycles are derived statistically from the stress response PSD, as described in the next section.

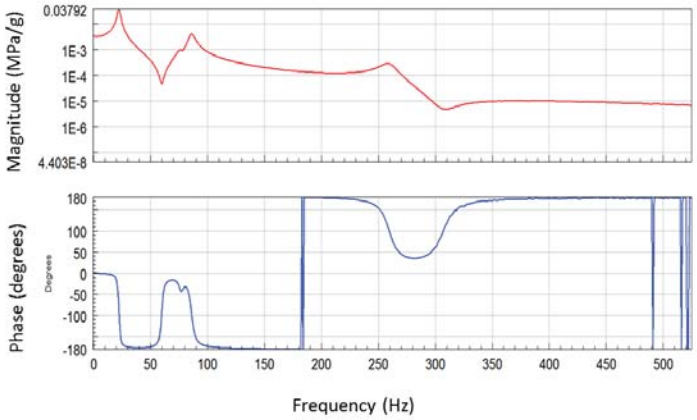

Figure 7: Stress FRF obtained at a critical node (3100).

For the time domain approach, a modal transient analysis is performed in ABAQUS to determine the modal response time histories for each loading condition. Stress time histories were obtained by modal superposition of the modal stresses with the modal coordinates using the commercial software nCode DesignLife^{TM}. This approach allows the size of the finite element result file to be kept small, since stress time histories at all nodes are not required, and those of interest can be generated quickly. The accuracy of the modal approach is dependent on the number of modes included in the analysis. In this study, the first 8 modes were used, covering natural frequencies up to 300 Hz. This selection was made based on the FRF at the critical node, shown in Figure 7, where it is seen that the main excited modes are all within the 0-300 Hz range.

3.4 Fatigue analyses

Fatigue damage can be calculated using frequency or time domain data [13, 14]. Both approaches are considered here in order to highlight differences between them.

Frequency Domain Fatigue Analysis

A common approach for characterizing random vibrations is to compute the ensemble averaged PSDs. This representation is useful because it enables identification of dominant frequency components, as well as the average energy level within each frequency band. With this approach, however, the PDF of stress cycle rainflow ranges must be derived from the stress PSD in order to estimate the fatigue life. There are a number of algorithms for doing so, several of which are supported by nCode DesignLife used in this work. The particular method used was given by Lalanne [15] and is based on the seminal work of Rice [16]. It is the most often used and can handle a wide range of loading conditions [13]. Rice demonstrated that for a signal of arbitrary bandwidth, the PDF of the peaks could be obtained from the weighted sum of the Rayleigh and Gaussian distributions. Lalanne reasoned that over a sufficiently long period of time, the PDF of rainflow ranges would tend to the PDF of the peaks and thereby demonstrated that Rice's original formula would also suffice for rainflow ranges.

The spectral fatigue method is robust, efficient and offers advantages over the time domain approach (next described) when limited stress time history data is available. However, this approach is only valid when the underlying random process is ergodic, stationary and Gaussian [13]. Here, an ergodic process is meant to describe a random process in which the time average of one sequence of events is the same as the ensemble average (and vice versa).

Time Domain Fatigue Analysis

In the time domain, time histories of stresses are directly counted using a rainflow cycle counting technique [17]. The damage from each cycle is then linearly summed using the

Palmgren-Miner [18, 19] damage accumulation law. The time domain approach is applicable to any type of signal, whether it be stochastic or deterministic. This approach, however, proves computationally intensive for stochastic loadings because long stress time histories are required to generate the tails of the stress range histogram in a statistically accurate manner. Poorly realized extremes can have a detrimental effect on the fatigue life estimate as the most damaging events are attributable to the high stress ranges in the tails. Convergence in damage estimates therefore improve with an increasing number of data points in a signal [13]. In many practical cases, it is simply not possible to obtain the required duration of time signal for accurate rainflow counting. In these cases especially, a frequency domain approach offers significantly more accurate fatigue life estimates under the aforementioned conditions.

3.5 Interpretation of the fatigue results

Contour plots of the fatigue damage obtained using the time domain method are shown in Figure 8 for the three loadings described in section 3.2. The critical node (3100) is the same in the three cases; it is in the top right radius and is represented by a small white marker on the plots in Figure 8. Note that a second critical point in the top left radius exists due to symmetry. Under the linear cumulative damage law, failure occurs when the damage equals unity. Thus, an accumulated damage of 10^{-8} for a 50 second exposure corresponds to an estimated fatigue life of $5x10^{9}$ seconds or roughly 158 years for that loading condition.

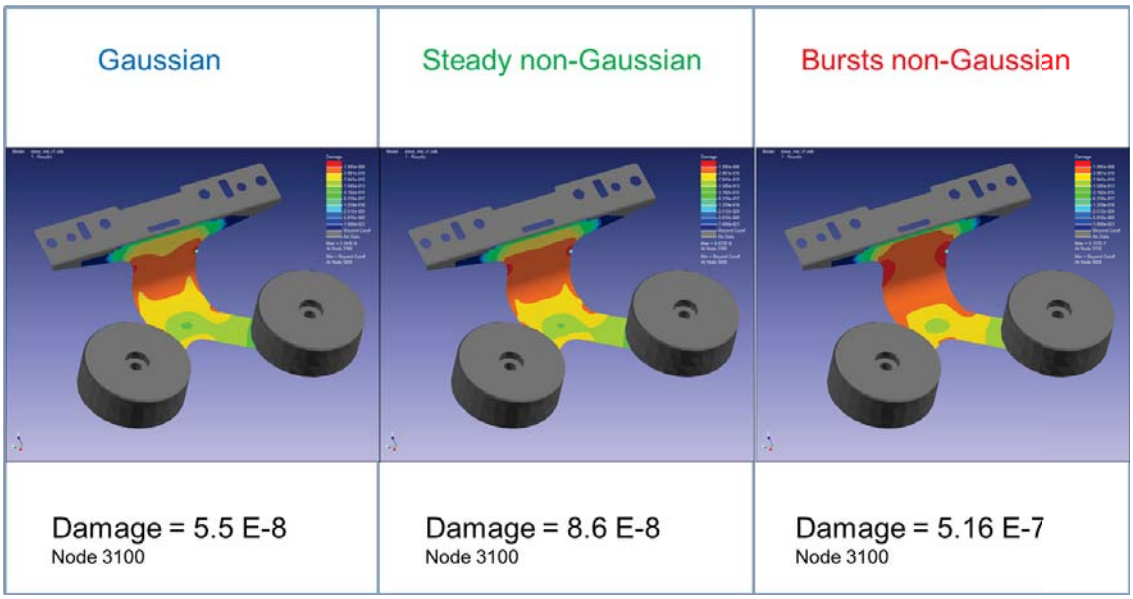

Figure 8: Contour plot of fatigue damage from various types of excitations.

Table 2 provides further evidence that the non-Gaussian load made of bursts is indeed the most severe. It is clear that leptokurtic input excitation signals are more damaging than Gaussian signals, even though all excitation signals share the same energy level. However, it is also clear that damage is not only related to the kurtosis of the input. Although the steady and bursts non-Gaussian signal have nearly the same kurtosis value of approximately 7, the damage resulting from their application is very different. The signal made of bursts clearly generates more damage in this example. This is due to the much higher maximum stress range. The steady non-Gaussian signal is approximately 1.5 times more damaging than the Gaussian stationary one, whereas the bursts non-Gaussian is over 9 times more severe in terms of fatigue. A plot of the stress range PDF is shown in Figure 9. Here, the higher stress ranges associated with the burst non-Gaussian loading are clearly evident.

Signal	Input RMS (g)	Input kurtosis	Output RMS (MPa)	Output kurtosis	Max Stress Range (MPa)	Max Damage
Normal	3.04	3	47.1	2.95	334	$5.5x10^{-8}$
Steady non-Gaussian	3.04	7.11	48.2	2.95	336	$8.6x10^{-8}$
Burst non-Gaussian	3.03	7.16	47.2	3.57	405	$5.16x10^{-7}$

Table 2: Comparison of stress response and accumulated damage for three loading conditions.

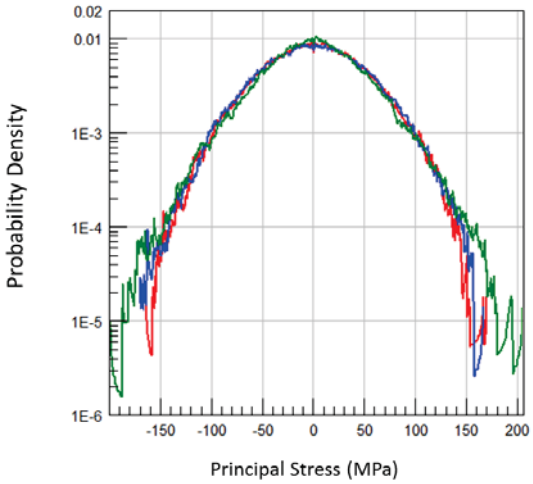

Figure 9: The PDFs of the stress response: Gaussian (red), steady non-Gaussian (blue) and burst non-Gaussian (green).

One can compare the time domain analysis and spectral domain analysis results to understand the differences between the approaches. The contour plot of damage resulting from the spectral domain fatigue analysis for the Gaussian case is illustrated in Figure 10. As expected, the spectral domain analysis gives a higher damage of $8.1x10^{-8}$ compared with $5.5x10^{-8}$ for the rainflow counting time domain method because the tails of the former are statistically better defined. A plot of the rainflow counting histograms for the Gaussian case using the two approaches clearly indicates this point, as shown in Figure 11.

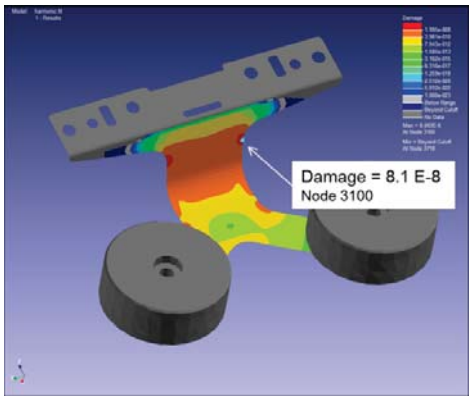

Figure 10: Contour plot of damage from an excitation defined as a PSD.

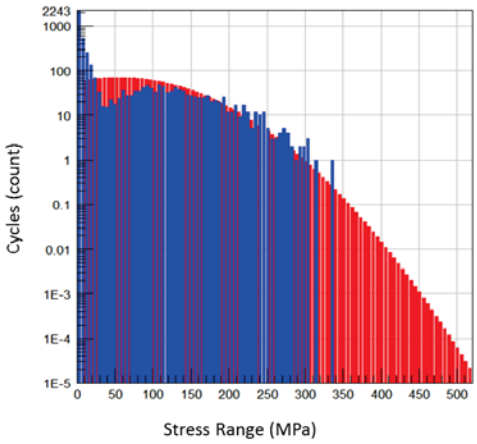

Figure 11: Rainflow histograms from time domain (blue) and spectral domain (red) for a 50 second exposure duration.

The correlation between the two approaches increases rapidly with signal duration as shown in Figure 12, where three longer realizations of Gaussian signals were considered: 100, 200 and 500 seconds It is clear that the damage computed from the time domain and spectral approaches converge to within 5% when the signal reaches 500 seconds. However, 500 seconds of simulated time for the time domain analysis is more computationally expensive than the spectral fatigue calculation.

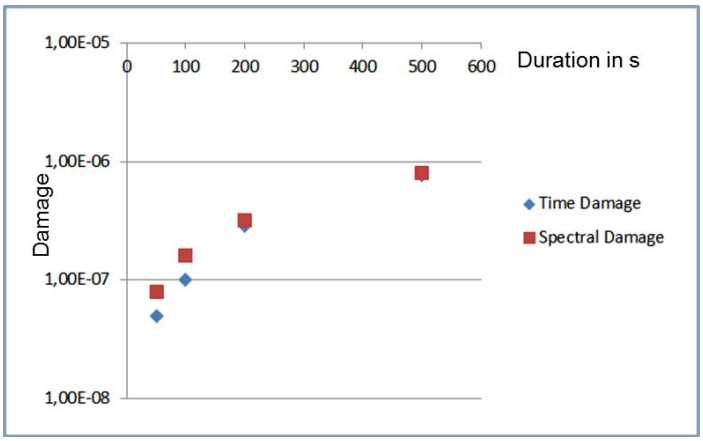

Figure 12: Comparison of damage from spectral and time approaches with duration of signal.

Finally, recall that the spectral fatigue approach is a robust, efficient and accurate way of estimating fatigue life when the underlying random process is Gaussian. This limitation stems from the assumption of a Gaussian process, which is used when the distribution of peaks is computed [2, 13, 15, 16]. An extension of the spectral fatigue approach for non-Gaussian processes has been studied and seems to give satisfactory results [8]. However, in order to apply it, it is necessary to evaluate the kurtosis of the stress response knowing the kurtosis of the load and the FRF. This is the subject of the next section.

4. MODELLING INPUT–OUTPUT STATISTICS

Expressions for the kurtosis of the stress response in terms of the kurtosis of the load and the frequency response of the system are next discussed for the cases of steady and burst non-Gaussian inputs. In the following, the structural response is assumed to be linear so that the structure can be modelled as a linear time-invariant (LTI) system.

4.1 Input–output kurtosis relationship in the case of a steady non-Gaussian input

For the steady non-Gaussian case, statistics of the output signal for a LTI system can be calculated using the cumulants [20]. Cumulants are alternatives to the statistical moments and have interesting properties such as additivity and homogeneity. Additivity means that the cumulants of the sum of n independent random variables are the sum of the cumulants of each random variable. Therefore, in the case of an independent and identically distributed (i.i.d.) process, cumulants are additive under convolution. Homogeneity means that if a random variable X is multiplied by a constant c, then the m^{th} cumulant of this product will be the m^{th} cumulant of X multiplied by c^m. Therefore, if the convolution is interpreted as a weighted sum of shifted copies of the input signal, the 2nd and 4th cumulants of the response signal c_{y2} and c_{y4} can be derived from the 2nd and 4th cumulants of the input signal c_{x2} and c_{x4} and from the coefficients h_i of the impulse response function as:

$$\begin{aligned} c_{y2} &= c_{x2}\sum h_i^2 \\ c_{y4} &= c_{x4}\sum h_i^4 \end{aligned} \tag{9}$$

The relationship between cumulants and moments are given by the Leonov and Shiryayev formulae [20] for the 2nd and 4th order cumulants c_{y2} and c_{y4} as a function of the 2nd and 4th order moments m_{y2} and m_{y4}. In the case of a zero-mean signal, these are:

$$\begin{aligned} c_{y2} &= m_{y2} \\ c_{y4} &= m_{y4} - 3{m_{y2}}^2 \end{aligned} \tag{10}$$

The output kurtosis is obtained by inserting equations (10) into equation (2) giving

$$\kappa_y = \frac{m_{y4}}{{m_{y2}}^2} = \frac{c_{y4}}{{c_{y2}}^2} + 3.0 \tag{11}$$

The output kurtosis of a zero-mean process expressed in terms of the impulse response and input kurtosis is obtained by substituting equations (9) into equation (11) giving

$$\kappa_y = \frac{\sum h_i^4}{\left(\sum h_i^2\right)^2}\left(\kappa_x - 3.0\right) + 3.0 \tag{12}$$

Now consider how the behavior of the output kurtosis is changed as a function of the characteristics of the impulse response function (IRF). The IRF corresponding to systems with very low damping will oscillate longer than the IRF corresponding to a highly damped system. In relation to equation (12), an IRF with long decaying oscillations will maximize the squared terms in the denominator compared to the terms raised to the 4th power in the numerator. This will lead to a lower output kurtosis for a lightly damped system than for a more heavily damped one. This behavior is consistent with the observation that the output kurtosis tends to Gaussian as the bandwidth of the filter, i.e, the amount of damping, decreases [1, 21].

Equation (12) is only valid for i.i.d. processes which have no temporal dependency and are spectrally flat. Equation (12) can be generalized to non-spectrally flat (colored) noise by considering the colored noise as a filtered version of spectrally flat noise, that is,

$$\kappa_y = \frac{\sum f_i^4}{\left(\sum f_i^2\right)^2}\frac{\left(\sum c_i^2\right)^2}{\sum c_i^4}\left(\kappa_x - 3.0\right) + 3.0 \tag{13}$$

where c_i are the values of the autocorrelation function of the input noise and f_i are the values of the convolution of the autocorrelation function with the IRF.

4.2 Input–output kurtosis relationship in the case of burst non-Gaussian input

Finding a closed-form solution for the burst non-Gaussian case is somewhat more complicated than the steady non-Gaussian case. The approach proposed here is one of

deduction and has been developed with the aid of numerical simulations. The numerical simulations were conducted by generating 20 different burst non-Gaussian signals and passing them through 15 filters of various bandwidths to deduce a relationship between the 'kurtosis rate' and the bandwidth. Here the 'kurtosis rate' represents the input-output kurtosis relationship and is defined for $\kappa_x \neq 3$ as:

$$\kappa_r = \frac{\kappa_y - 3}{\kappa_x - 3} \tag{14}$$

Simulations have shown that the kurtosis rate fluctuates between 0 and 1, which means that the kurtosis of the output signal varies between 3.0 and the kurtosis of the input signal.

The behavior of the 'kurtosis rate' can be explained in terms of the time required for the system IRF to decrease to some fraction of its initial amplitude, t_f, and the period of the bursts, T_a. In this work, a fraction of 0.1 was used for t_f. If the IRF is very short compared to the period of bursts T_a in the input signal, then each block is filtered independently and the output signal will just be the filtered stationary part of the input signal, modulated with the same periodic waveform $a(t)$. In this case, the kurtosis of the output signal will equal that of the input signal. Numerical simulations have shown that considering t_f smaller than $1/10^{th}$ of the period of bursts in the input signal results in an output kurtosis similar, if not equal, to the input kurtosis, that is, a 'kurtosis rate' of 1. Thus, $t_f \leq 0.1T_a$ is a general criterion for the input kurtosis to be reproduced in the output.

If the IRF is very long compared to the period of bursts T_a in the input signal, the convolution process will average out the high amplitude excursions. In this case, the output distribution tends towards a Gaussian distribution by virtue of the Central Limit Theorem [1, 22]. Hence, the 'kurtosis rate' becomes 0. It is interesting to note that a burst non-Gaussian signal is similar to cyclostationary noise [23], which is formed by a stationary noise $x(t)$, multiplied by a waveform $a(t)$ of period $T_a = 1/f_a$, where f_a is the cyclic frequency of oscillator $a(t)$. In this case, the stationary process $x(t)$ is supposed Gaussian. Authors from the electronics industry have shown that filtering a cyclostationary noise process with cyclic frequency f_a through a LTI band-pass filter (with bandwidth $B < f_a/2$) results in stationary output noise [24]. The present case of burst noise is a bit different than cyclostationary noise as the periodic wave is generally made of variable amplitudes overlapping weighting windows. Here, numerical simulations have shown that considering $t_f > 4T_a$ is a robust criterion for the output signal to become stationary and Gaussian, no matter what the input kurtosis was.

Finally, if the IRF length lies somewhere between these extremes, that is, if $0.1T_a < t_f \leq 4T_a$, then a linear-logarithmic interpolation is adopted. To summarize, the 'kurtosis rate' law is expressed as:

$$\kappa_r = \frac{\kappa_y - 3.0}{\kappa_x - 3.0} = \begin{cases} 0 & t_f / T_a > 4 \\ \dfrac{\log(4) - \log(t_f / T_a)}{\log(4) + 1} & 0.1 > t_f / T_a \leq 4 \\ 1 & t_f / T_a \leq 0.1 \end{cases} \tag{15}$$

Equation (15) shows that the kurtosis of the output signal tends to 3.0 as the bandwidth of the filter decreases. Equation (15) also illustrates that the full input kurtosis can be passed to the output if the input signal is modulated with a sufficiently low frequency carrier.

4.3 Comparison with simulation

Simulations have shown different damage values for the steady and burst non-Gaussian input loads, although both input signals had the same energy and kurtosis. The difference in

damage is due to the response kurtosis being higher in the case of a burst non-Gaussian signal. In this section, the kurtosis input-output relationships found in the two previous sections will be used to retrieve the statistics obtained by FE time domain simulation. The FE simulation is described in section 3.

Both relationships are based on the IRF of the system. The IRF relating output stress to input acceleration at the critical node is obtained by taking the inverse Fourier transform of the FRF shown in Figure 7. The obtained IRF is shown in Figure 13. It has the classical form of a decaying exponential and the decay rate is driven by the amount of damping.

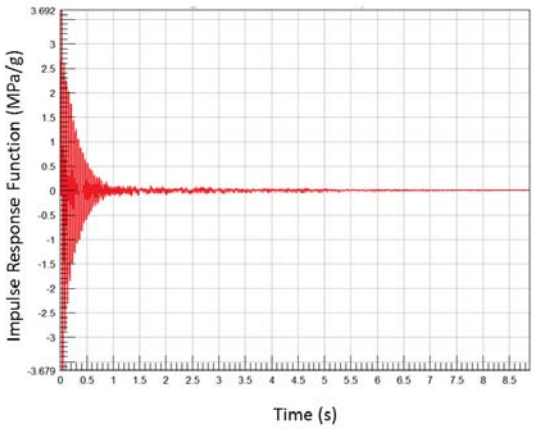

Figure 13: Impulse response function obtained from stress FRF at a critical node (3100).

Let us look first at the steady non-Gaussian loading signal, which is presented in section 3.2. Equation (13) can be used to predict the kurtosis of the stress response and this leads to a predicted value of 3 compared to a 'measured' value of 2.95. Here, the measured value is that computed from the simulated time domain response calculation.

Now consider the burst loading signal, which is also presented in section 3.2. There are roughly 4 bursts per seconds, which means that the period of bursts T_a is 0.25. The IRF at the critical node takes 0.65 seconds to reach $1/10^{th}$ of its initial amplitude. From equation (15), the kurtosis rate is 0.11 and since the kurtosis of the excitation is 7.16, the predicted kurtosis of the stress response is 3.45. This is close to the measured value 3.57.

The above results demonstrate that equations (13) and (15) can be used to predict the kurtosis of the stress output for a LTI system exposed to steady and burst non-Gaussian loadings, respectively. Together with the work of Benasciutti and Tovo [8], spectral fatigue life estimates based on the kurtosis of the excitation and characteristics of the LTI system are possible. A demonstration of this is left as an area of future work.

5. CONCLUDING REMARKS

The fatigue life of an automotive horn bracket was investigated to determine how changes in the loading kurtosis influence the results. Three base acceleration loadings having the same PSD and RMS level, but different kurtosis were considered: a Gaussian loading and two leptokurtic non-Gaussian loadings of a steady and burst nature. Using results from a computationally intensive time domain analysis, it was found that burst non-Gaussian loading produced the most damage, followed by the steady non-Gaussian loading and lastly the Gaussian loading.

In the case of non-Gaussian loads, the stress response may tend to Gaussian depending on type of non-Gaussian input signal and on the bandwidth of the system's frequency response. Non–stationary processes with bursts of energy spaced in time easily propagate their leptokurtic nature to the response. The more bursts are separated in time, the more input kurtosis will be transferred to the output response. On the contrary, steady non-Gaussian

processes essentially produce responses that tend to Gaussian, especially for narrow band systems.

An alternative spectral fatigue analysis was undertaken for the Gaussian loading condition. The spectral fatigue analysis is considered more attractive, when applicable, than the time domain approach because long time histories are needed to generate statistically accurate stress distributions in the latter. The two approaches were shown to converge when the time domain simulation was carried out over an extended period. However, the standard spectral fatigue analysis is considered valid only for Gaussian processes. In the case of leptokurtic processes, it is anticipated that the standard spectral fatigue analysis under-estimates damage.

An extension of the spectral fatigue analysis for non-Gaussian processes has been studied [8], but requires knowledge of the kurtosis of the stress response. Formulations for the kurtosis of the stress response in terms of the kurtosis of the load and the FRF were given for both the steady and the burst non-Gaussian load types. These were validated using time domain simulations of the stress response. Predictions of fatigue life using this new approach will be considered in future work.

Finally, the excitations considered in this work were such that maximum stress range was below the yield stress of 400 MPa. However, higher loading levels could result in material and/or large-deflection nonlinearities. An assessment of the applicability of the spectral fatigue analysis, or development of some approximate form thereof, would need to be undertaken under such conditions. However, such an endeavour is beyond the scope of the present effort.

ACKNOWLEDGMENTS

The authors would like to acknowledge Paul Hollingsworth from Jaguar Land Rover, UK for the FE model.

REFERENCES

[1] Rizzi, S.A., Przekop, A., and Turner, T.L., "On the response of a nonlinear structure to high kurtosis non-Gaussian random loadings," *EURODYN 2011, 8th International Conference on Structural Dynamics*, Paper 41, Leuven, Belgium, July 4-6, 2011.

[2] Newland, D.E., *An introduction to random vibrations and spectral analysis (2nd edition)*. New York, Longman Inc, 1984.

[3] Smallwood, D.O., "Vibration with non-Gaussian noise," *Journal of the Institute of Environmental Sciences and Technology*, Vol. 52, No. 3, pp. 13-30, 2009.

[4] Sweitzer, K.A., "Random vibration response statistics for fatigue analysis of nonlinear structures," Ph.D. Dissertation, Institute of Sound and Vibration Research, University of Southampton, UK, 2006.

[5] Papoulis, A., *Probability, random variables, and stochastic processes (3rd edition)*, McGraw-Hill, Inc., 1991.

[6] S.R., W., "Nonlinear vibration models for extremes and fatigue," *ASCE Journal of Engineering Mechanics*, Vol. 114, No. 10, pp. 1772-1790, 1988.

[7] Ochi, M.K. and Ahn, K., "Probability distribution applicable to non-Gaussian random processes," *Probabilistic Engineering Mechanics*, Vol. 9, pp. 255-264, 1994.

[8] Benasciutti, D. and Tovo, R., "Cycle distribution and fatigue damage assessment in broad-band non-Gaussian random processes," *Probabilistic Engineering Mechanics*, Vol. 20, pp. 115-127, 2005.

[9] Steinwolf, A., "Two methods for random shaker testing with low kurtosis," *Sound & Vibration*, pp. 18-22, October, 2008.

[10] "ABAQUS online documentation, ABAQUS analysis user's manual." Providence, RI: Dassault Systemes Simulia Corp., 2012.

[11] "MIL-STD-810F: Test method standard for environmental engineering considerations and laboratory tests," United States Department of Defense, 2000.

[12] Matsuishi, M. and Endo, T., "Fatigue of metals subjected to varying stress," *Japan Society of Mechanical Engineers*, Fukuoka, Japan, March, 1968.
[13] Halfpenny, A., "Rainflow cycle counting and fatigue analysis from PSD," *Proceedings of the ASTELAB Conference*, Paris, France, September 25 – 27, 2007.
[14] "nCode DesignLife theory guide," HBM-nCode Products, Rotherham, UK 2009.
[15] Lalanne, C., "Mechanical vibration & shock (volume 4)," Hermes Penton Ltd, London 2002.
[16] Rice, S.O., "Mathematical analysis of random noise," *Bell System Technical Journal*, Vol. 23, pp. 282-332, 1944.
[17] Downing, S.D. and Socie, D.F., "Simple rainflow counting algorithms," *International Journal of Fatigue*, Vol. 4, No. 1, pp. 31-40, 1982.
[18] Palmgren, A., "The service life of ball bearings," NASA Technical Translation TT F-13460 (Translation of "Die lebensdauer von kugellagern," Zeitschrift des Vereines Deutscher Ingenierure, Vol. 68, No. 14, pp. 339-341, 1924), 1971.
[19] Miner, M.A., "Cumulative damage in fatigue," *Trans. ASME, Journal of Applied Mechanics*, Vol. 67, pp. A159-A164, 1945.
[20] Lacoume, J.-L., Amblard, P.-O., and Comon, P., *Statistiques d'ordre supérieur pour le traitement du signal*, Masson, 1997.
[21] Papoulis, A., "Narrow-band systems and Gaussianity," *IEEE Transactions on Information Theory*, Vol. 18, No. 1, pp. 20-27, 1972.
[22] Bendat, J.S. and Piersol, A.G., *Random data: Analysis and measurement procedures*, Wiley-Interscience, 1971.
[23] Gardner, W.A., *Introduction to random processes with applications to signals and systems (2nd edition)*, McGraw-Hill, 1989.
[24] Roychowdhury, J., Long, D., and Feldman, P., "Cyclostationary noise analysis of large RF Circuits with multi-tone excitation," *IEEE Journal of Solid-State Circuits*, Vol. 33, pp. 324-336, 1998.